Possible antimagnetic rotational band and neutron alignment in ^{113}In

K. Y. Ma (马克岩),[1,2] J. B. Lu (陆景彬),[1,*] J. Li (李剑),[1] D. Yang (杨东),[1] Y. J. Ma (马英君),[1] W. J. Sun (孙无忌),[1] X. Guan (管弦),[1] D. M. Zhang (张大明),[2] L. H. Zhu (竺礼华),[3] X. G. Wu (吴晓光),[4] Y. Zheng (郑云),[4] C. B. Li (李聪博),[4] and Y. Z. Liu (刘运祚)[1]

[1]*College of Physics, Jilin University, Changchun 130012, China*

[2]*College of Electronic Science & Engineering, Jilin University, Changchun 130012, China*

[3]*School of Physics and Nuclear Energy Engineering, Beihang University, Beijing 100191, China*

[4]*China Institute of Atomic Energy, Beijing 102413, China*

(Received 18 March 2019; revised manuscript received 11 April 2019; published 31 July 2019)

High-spin states of ^{113}In have been populated using the ^{110}Pd(^{7}Li, $4n$)^{113}In reaction at beam energies of 38 and 50 MeV. More than 50 new γ transitions are observed in ^{113}In. Three previously observed magnetic dipole bands are extended to higher spin states, and several new $E2$ crossover transitions within the bands are observed in two of the dipole bands. A new positive-parity $\Delta I = 2$ band built on the $\pi d_{5/2}$ configuration is established. The known $\Delta I = 2$ band is extended to $51/2^+$ state, and a gentle up-bend associated to the alignment of neutrons in the normal-parity $\nu g_{7/2}/d_{5/2}$ orbitals is found. The properties of this band are discussed based on the self-consistent tilted axis cranking relativistic mean-field model calculations. The predicted $B(E2)$, deformation parameters β_2 and γ, and $J^{(2)}/B(E2)$ ratios indicate that the $\Delta I = 2$ band based on the $\pi g_{9/2}^{-2} g_{7/2} \otimes \nu(h_{11/2})^2$ and $\pi g_{9/2}^{-2} g_{7/2} \otimes \nu(h_{11/2})^2 (g_{7/2}/d_{5/2})^2$ configurations, has the characteristics of antimagnetic rotation. Furthermore, the two-shears-like mechanism for the possible antimagnetic rotational bands is examined by investigating the orientation of the angular momenta.

DOI: 10.1103/PhysRevC.100.014326

I. INTRODUCTION

The study of antimagnetic rotation has been a topic of great interest in weakly deformed or nearly spherical nuclei in the past few years. The explanation of such bands in terms of the two-shears-like mechanism was first proposed by Frauendorf [1]. In this interpretation, the two proton angular momentum vectors are pointing opposite to each other and are nearly perpendicular to the orientation of the total angular momentum vector of the valence neutrons at the band head. They form the blades of the two shears. An increase in the total angular momentum is generated by the simultaneous closing of the two proton blades along the direction of the total angular momentum vector, while the direction of the total angular momentum stays unchanged. Furthermore, the phenomenon of antimagnetic rotation is characterized by the appearance of the weak $E2$ transitions reflecting the weakly deformed core, a decrease of the $B(E2)$ values with increasing spin, and a large $J^{(2)}/B(E2)$ ratio [1].

Experimentally, most of the antimagnetic rotational bands were reported in Cd [2–8] and Pd [9–14] isotopes in the $A \approx 110$ mass region. In particular, in the Cd isotopes, more than seven antimagnetic rotational bands based on the high-Ω $g_{9/2}$ proton holes and low-Ω $h_{11/2}$, $g_{7/2}/d_{5/2}$ neutron orbitals, have been observed in ^{105}Cd [2], ^{106}Cd [3], ^{107}Cd [4], ^{108}Cd [5,6], ^{109}Cd [7], and ^{110}Cd [8] nuclei. However, the experimental study of antimagnetic rotation in the neighboring indium isotopes is scarce. So far, the conclusive experimental evidence of antimagnetic rotation has only been reported in three indium isotopes, namely, ^{108}In [15], ^{110}In [15], and ^{112}In [16,17]. Therefore, it is interesting to investigate the systematic properties of antimagnetic rotation along indium isotopic chain. For this purpose, we try to extend the study of antimagnetic rotation to neighboring isotope ^{113}In.

II. EXPERIMENTAL DETAILS

High-spin states in ^{113}In were populated in two complementary experiments, both of which employed the ^{110}Pd, (^{7}Li, $4n$)^{113}In reaction. Two experiments were undertaken with the HI-13 tandem accelerator at CIAE in Beijing. For the first experiment, the target was prepared by evaporating 2.4 mg/cm^2 of 97.2% enriched ^{110}Pd on 0.4 mg/cm^2 ^{197}Au foil. The ^{7}Li beam was provided by the HI-13 tandem accelerator, and delivered at a beam energy of 50 MeV. This beam energy was chosen to favor the population of high angular momentum and high excited states in ^{113}In. A total of 1.9×10^8 γ-γ coincidence events were recorded. For the second experiment, the ^{110}Pd target, with an enrichment of 97.2% and a thickness of 1.1 mg/cm^2, was rolled onto an Au backing. The bombarding energy of 38 MeV was selected to populate the nucleus ^{113}In by the excitation function measurements, which favored the study of medium and low spins in ^{113}In. A total of 1.5×10^8 twofold coincidence events were collected.

γ-γ coincidence measurements were performed using the detecting system consisting of 12 Compton-suppressed HPGe

*ljb@jlu.edu.cn

 ©2019 American Physical Society

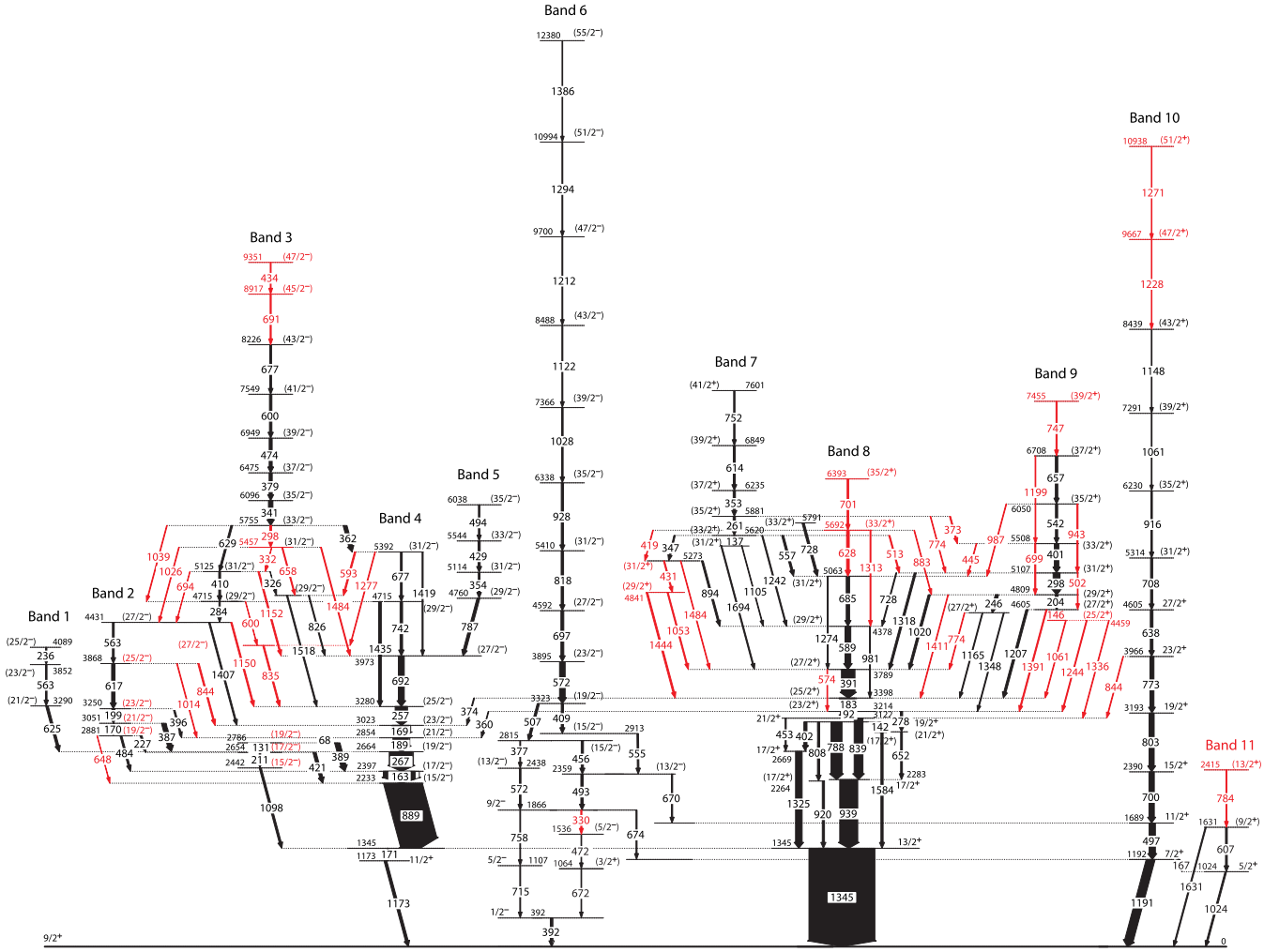

FIG. 1. Level scheme of ^{113}In deduced from the present work. Transition energies are given in keV and their measured relative intensities are proportional to the widths of the arrows. New transitions and levels are marked as red.

detectors and two planar HPGe detectors. In our array, the Ge detectors were placed at 90°, ±37°, ±30°, and ±60° relative to the beam direction. Each HPGe detector had an efficiency of approximately 35% of the standard 7.6 × 7.6 cm NaI(Tl) crystal. The recorded γ-γ coincidence events are about 1500 per second in our array. Energy and efficiency calibrations of the detectors were performed by standard sources of ^{60}Co and ^{152}Eu. A symmetrized coincidence matrix and a asymmetric DCO (directional correlation ratios of oriented states) matrix [18] were constructed for off-line analysis. The DCO matrix was created by sorting the detectors at ±37° on one axis and the detectors at 90° on the other. In our array geometry, if one gates on a quadrupole transition, the expected $R_{\rm DCO}$ value is close to 1.0 for stretched $E2$ transitions and close to 0.6 for stretched dipole transitions. Similarly, with a dipole gating transition, the $R_{\rm DCO}$ value is close to 1.7 and 1.0 for quadrupole and dipole transitions, respectively.

III. RESULTS

The level scheme of ^{113}In deduced from the present study is shown in Fig. 1. Properties and placements of all γ rays are listed in Table I. In this work, 11 bands are observed and labeled 1-11 to facilitate discussion. Among them, bands 1, 2, 4, 6, 8, and 10 have previously been reported by Chakrawarthy *et al.* [19] and Naguleswaran *et al.* [20]. Subsequently, bands 3, 5, 7, and 9 have been observed and suggested as candidate magnetic rotational bands in our early works [21,22]. In the present work, the high-spin states of ^{113}In are reinvestigated via two experiments. One experiment with beam energy of 50 MeV has been done in 2012 [21], the other one with beam energy of 38 MeV is a new experiment. Compared with the results reported in Refs. [19–22], the level scheme of ^{113}In is extended and modified with the addition of more than 50 new γ transitions. For instance, a new $\Delta I = 2$ band is established, and several additional in-band and interband transitions are identified. The relevant details of current level scheme will be described below.

Band 2 was observed by Chakrawarthy *et al.* [19]. However, the spin-parity assignments of the levels in band 2 are absent. In the current work, several new linking transitions between bands 2 and 4 are identified. Multipolarity analysis indicates that the 1014 and 1407 keV linking transitions are of $\Delta I = 2$ character with DCO ratios of 1.75 and 1.68

TABLE I. Energies, initial and final excitation energies, relative intensities, DCO ratios, initial and final state spins, and multipolarities for transitions assigned to ^{113}In in the present series of experiments.

E_γ[a] (keV)	E_i (keV)	E_f (keV)	$I\gamma$[b]	$R_{\rm DCO}$[c]	$R_{\rm DCO}$[d]	$J_i^\pi \rightarrow J_f^\pi$	Multipolarity
50.5	3122	3072	25(5)	0.72(29)	1.21(48)	$21^+/2 \rightarrow 19^+/2$	$(M1/E2)$
68.4	2854	2786				$(21^-/2) \rightarrow (19^-/2)$	$(M1/E2)$
92.2	3214	3122	145(7)	0.61(12)	1.07(21)	$(23^+/2) \rightarrow 21^+/2$	$(M1/E2)$
131.7	2786	2654	39(8)		1.05(28)	$(19^-/2) \rightarrow (17^-/2)$	$(M1/E2)$
137.1	5620	5483	20(5)		1.07(42)	$(33^+/2) \rightarrow (31^+/2)$	$(M1/E2)$
142.5	3072	2929	21(5)		1.09(44)	$19^+/2 \rightarrow (17^+/2)$	$(M1/E2)$
146.0	4605	4459	18(6)		1.05(42)	$(27^+/2) \rightarrow (25^+/2)$	$(M1/E2)$
163.4	2397	2233	482(15)	0.58(6)	0.97(10)	$(17^-/2) \rightarrow (15^-/2)$	$(M1/E2)$
167.0	1192	1024	30(7)	0.64(19)		$7^+/2 \rightarrow 5^+/2$	$(M1/E2)$
169.6	3023	2854	265(10)	0.61(7)	1.03(12)	$(23^-/2) \rightarrow (21^-/2)$	$(M1/E2)$
170.2	3051	2881	45(9)		0.95(26)	$(21^-/2) \rightarrow (19^-/2)$	$(M1/E2)$
171.5	1345	1173	15(5)		1.11(44)	$13^+/2 \rightarrow 11^+/2$	$M1/E2$
183.5	3398	3214	239(7)	0.72(10)		$(25^+/2) \rightarrow (23^+/2)$	$(M1/E2)$
189.6	2854	2664	235(7)	0.61(8)	1.05(13)	$(21^-/2) \rightarrow (19^-/2)$	$(M1/E2)$
199.4	3250	3051	41(8)		1.02(27)	$(23^-/2) \rightarrow (21^-/2)$	$(M1/E2)$
203.7	4809	4605	52(9)		1.12(28)	$(29^+/2) \rightarrow (27^+/2)$	$(M1/E2)$
211.4	2654	2442	21(5)		0.97(38)	$(17^-/2) \rightarrow (15^-/2)$	$(M1/E2)$
226.8	2881	2654	27(6)		1.04(36)	$(19^-/2) \rightarrow (17^-/2)$	$(M1/E2)$
236.3	4089	3852	19(6)		1.07(43)	$(25^-/2) \rightarrow (23^-/2)$	$(M1/E2)$
246.1	4809	4563	46(9)		0.88(22)	$(29^+/2) \rightarrow (27^+/2)$	$(M1/E2)$
257.1	3280	3023	181(6)	0.61(10)		$(25^-/2) \rightarrow (23^-/2)$	$(M1/E2)$
261.0	5881	5620	50(10)		1.03(26)	$(35^+/2) \rightarrow (33^+/2)$	$(M1/E2)$
267.6	2664	2397	355(12)	0.63(8)		$(19^-/2) \rightarrow (17^-/2)$	$(M1/E2)$
278.5	3214	2936	61(12)	0.61(15)		$(23^+/2) \rightarrow (21^+/2)$	$(M1/E2)$
284.5	4715	4431	15(5)		1.06(42)	$(29^-/2) \rightarrow (27^-/2)$	$(M1/E2)$
297.8	5755	5457	12(4)		1.11(44)	$(33^-/2) \rightarrow (31^-/2)$	$(M1/E2)$
298.1	5107	4809	90(13)		1.01(19)	$(31^+/2) \rightarrow (29^+/2)$	$(M1/E2)$
326.3	5125	4799	<10		1.05(47)	$(31^-/2) \rightarrow (29^-/2)$	$(M1/E2)$
330.0	1866	1536	14(5)	1.08(45)		$9^-/2 \rightarrow (5^-/2)$	$(E2)$
331.5	5457	5125	<10			$(31^-/2) \rightarrow (31^-/2)$	$(M1/E2)$
341.1	6096	5755	85(13)		1.08(23)	$(35^-/2) \rightarrow (33^-/2)$	$(M1/E2)$
347.5	5620	5273	12(4)		1.12(49)	$(33^+/2) \rightarrow (31^+/2)$	$(M1/E2)$
353.4	6235	5881	35(8)		1.05(29)	$(37^+/2) \rightarrow (35^+/2)$	$(M1/E2)$
354.1	5114	4760	25(6)		0.95(33)	$(31^-/2) \rightarrow (29^-/2)$	$(M1/E2)$
360.2	3214	2854	<10		1.13(50)	$(23^+/2) \rightarrow (21^-/2)$	(E1)
362.3	5755	5392	64(12)		1.09(26)	$(33^-/2) \rightarrow (31^-/2)$	$(M1/E2)$
373.2	5881	5508	<10			$(35^+/2) \rightarrow (33^+/2)$	$(M1/E2)$
374.2	3398	3023	<10		0.97(44)	$(25^+/2) \rightarrow (23^-/2)$	(E1)
377.5	2815	2438	28(7)	0.62(19)		$(15^-/2) \rightarrow (13^-/2)$	$(M1/E2)$
379.1	6475	6096	61(11)		1.04(25)	$(37^-/2) \rightarrow (35^-/2)$	$(M1/E2)$
386.8	3051	2664	69(12)		1.02(24)	$(21^-/2) \rightarrow (19^-/2)$	$(M1/E2)$
389.0	2786	2397	78(12)		0.98(22)	$(19^-/2) \rightarrow (17^-/2)$	$(M1/E2)$
391.1	3789	3398	201(7)	0.63(9)		$(27^+/2) \rightarrow (25^+/2)$	$(M1/E2)$
391.8	392	0				$1^-/2 \rightarrow 9^+/2$	
396.6	3250	2854	21(5)		1.06(42)	$(23^-/2) \rightarrow (21^-/2)$	$(M1/E2)$
401.1	5508	5107	48(10)		0.98(25)	$(33^+/2) \rightarrow (31^+/2)$	$(M1/E2)$
402.2	3072	2669	28(7)		1.02(30)	$19^+/2 \rightarrow 17^+/2$	$M1/E2$
409.5	3323	2913	24(6)	1.04(36)		$(19^-/2) \rightarrow (15^-/2)$	(E2)
409.8	5125	4715	28(7)		1.07(33)	$(31^-/2) \rightarrow (29^-/2)$	$(M1/E2)$
419.0	5692	5273	<10			$(33^+/2) \rightarrow (31^+/2)$	$(M1/E2)$
420.6	2654	2233	47(9)		1.01(25)	$(17^-/2) \rightarrow (15^-/2)$	$(M1/E2)$
429.1	5544	5114	32(7)		1.18(35)	$(33^-/2) \rightarrow (31^-/2)$	$(M1/E2)$
431.4	5273	4841	14(4)		1.05(44)	$(31^+/2) \rightarrow (29^+/2)$	$(M1/E2)$
433.8	9351	8917	18(5)		1.11(44)	$(47^-/2) \rightarrow (45^-/2)$	$(M1/E2)$
445.0	5508	5063	<10			$(33^+/2) \rightarrow (31^+/2)$	$(M1/E2)$
452.8	3122	2669	19(5)		1.64(66)	$21^+/2 \rightarrow 17^+/2$	E2

TABLE I. (Continued).

E_γ[a] (keV)	E_i (keV)	E_f (keV)	$I\gamma$[b]	$R_{\rm DCO}$[c]	$R_{\rm DCO}$[d]	$J_i^\pi \rightarrow J_f^\pi$	Multipolarity
456.5	2815	2359	26(7)	0.54(17)	1.30(41)	$(15^-/2) \rightarrow (13^-/2)$	$(M1/E2)$
472.0	1536	1064	<10			$(5^-/2) \rightarrow (3^+/2)$	(E1)
474.2	6949	6475	62(11)		1.13(27)	$(39^-/2) \rightarrow (37^-/2)$	$(M1/E2)$
484.1	2881	2397	27(7)		1.05(32)	$(19^-/2) \rightarrow (17^-/2)$	$(M1/E2)$
493.0	2359	1866	35(8)	1.03(29)	1.73(48)	$(13^-/2) \rightarrow 9^-/2$	E2
494.2	6038	5544	18(5)		1.20(48)	$(35^-/2) \rightarrow (33^-/2)$	$(M1/E2)$
497.5	1689	1192	95(10)		1.64(34)	$11^+/2 \rightarrow 7^+/2$	$E2$
501.8	5107	4605	10(3)		1.79(80)	$(31^+/2) \rightarrow (27^+/2)$	$(E2)$
507.4	3323	2815	34(8)	1.07(31)		$(19^-/2) \rightarrow (15^-/2)$	$E2$
513.5	5620	5107	<10			$(33^+/2) \rightarrow (31^+/2)$	$(M1/E2)$
542.1	6050	5508	40(9)		0.94(26)	$(35^+/2) \rightarrow (33^+/2)$	$(M1/E2)$
554.6	2913	2359	15(5)	0.57(23)		$(15^-/2) \rightarrow (13^-/2)$	$(M1/E2)$
557.1	5620	5063	22(6)		0.96(37)	$(33^+/2) \rightarrow (31^+/2)$	$(M1/E2)$
562.7	3852	3290	11(6)		0.95(36)	$(23^-/2) \rightarrow (21^-/2)$	$(M1/E2)$
563.1	4431	3868	16(7)		0.91(28)	$(23^-/2) \rightarrow (21^-/2)$	$(M1/E2)$
572.0	3895	3323	85(9)	0.94(19)		$(23^-/2) \rightarrow (19^-/2)$	$(E2)$
572.2	2438	1866	12(4)	1.09(48)		$(13^-/2) \rightarrow 9^-/2$	$(E2)$
574.5	3789	3214	10(3)		1.77(80)	$(27^+/2) \rightarrow (23^+/2)$	$(E2)$
589.5	4378	3789	87(9)		1.05(22)	$(29^+/2) \rightarrow (27^+/2)$	$(M1/E2)$
593.0	5392	4799	<10			$(31^-/2) \rightarrow (29^-/2)$	$(M1/E2)$
599.7	4715	4116	<10			$(29^-/2) \rightarrow (27^-/2)$	$(M1/E2)$
600.2	7549	6949	54(11)		1.04(25)	$(41^-/2) \rightarrow (39^-/2)$	$(M1/E2)$
607.0	1631	1024	20(5)	1.04(41)		$(9^+/2) \rightarrow 5^+/2$	$(E2)$
614.4	6849	6235	25(6)		1.08(38)	$(39^+/2) \rightarrow (37^+/2)$	$(M1/E2)$
617.5	3868	3250	51(10)		1.01(25)	$(25^-/2) \rightarrow (23^-/2)$	$(M1/E2)$
625.4	3290	2664	37(9)		1.11(31)	$(21^-/2) \rightarrow (19^-/2)$	$(M1/E2)$
628.5	5692	5063	38(9)		1.02(28)	$(33^+/2) \rightarrow (31^+/2)$	$(M1/E2)$
629.1	5755	5125	12(4)		1.04(45)	$(33^-/2) \rightarrow (31^-/2)$	$(M1/E2)$
638.1	4605	3966	40(9)	1.02(28)		$27^+/2 \rightarrow 23^+/2$	$E2$
647.6	2881	2233	<10			$(19^-/2) \rightarrow (15^-/2)$	$(E2)$
652.4	2936	2283	72(11)	1.08(24)		$(21^+/2) \rightarrow 17^+/2$	$(E2)$
657.5	6708	6050	53(10)		0.90(22)	$(37^+/2) \rightarrow (35^+/2)$	$(M1/E2)$
658.0	5457	4799	<10			$(31^-/2) \rightarrow (29^-/2)$	$(M1/E2)$
670.1	2359	1689	19(5)	0.75(30)	1.18(47)	$(13^-/2) \rightarrow 11^+/2$	$(E1)$
672.0	1064	392	<10			$(3^+/2) \rightarrow 1^-/2$	$(E1)$
674.4	1866	1192	16(5)	0.70(29)	0.97(41)	$9^-/2 \rightarrow 7^+/2$	
676.8	5392	4715	27(7)		1.01(31)	$(31^-/2) \rightarrow (29^-/2)$	$(M1/E2)$
677.1	8226	7549	35(8)		1.07(30)	$(43^-/2) \rightarrow (41^-/2)$	$(M1/E2)$
684.6	5063	4378	51(10)		0.98(25)	$(31^+/2) \rightarrow (29^+/2)$	$(M1/E2)$
691.0	8917	8226	27(7)		1.12(36)	$(45^-/2) \rightarrow (43^-/2)$	$(M1/E2)$
692.5	3973	3280	89(9)		1.03(22)	$(27^-/2) \rightarrow (25^-/2)$	$(M1/E2)$
694.3	5125	4431	<10			$(31^-/2) \rightarrow (27^-/2)$	(E2)
697.1	4592	3895	39(8)	1.03(28)		$(27^-/2) \rightarrow (23^-/2)$	(E2)
699.0	5508	4809	11(4)		1.67(73)	$(33^+/2) \rightarrow (29^+/2)$	(E2)
700.6	2390	1689	81(8)	1.02(22)		$15^+/2 \rightarrow 11^+/2$	E2
701.0	6393	5692	15(5)		1.07(45)	$(35^+/2) \rightarrow (33^+/2)$	$(M1/E2)$
708.7	5314	4605	32(7)	1.05(31)		$(31^+/2) \rightarrow 27^+/2$	(E2)
715.1	1107	392	13(4)	0.95(40)		$5^-/2 \rightarrow 1^-/2$	E2
728.1	5791	5063	30(7)		1.12(34)	$(33^+/2) \rightarrow (31^+/2)$	$(M1/E2)$
728.5	5107	4378	12(4)		1.17(51)	$(31^+/2) \rightarrow (29^+/2)$	$(M1/E2)$
742.5	4715	3973	38(9)		1.02(28)	$(29^-/2) \rightarrow (27^-/2)$	$(M1/E2)$
747.0	7455	6708	18(5)		1.09(44)	$(39^+/2) \rightarrow (37^+/2)$	$(M1/E2)$
752.3	7601	6849	12(4)		0.97(42)	$(41^+/2) \rightarrow (39^+/2)$	$(M1/E2)$
758.8	1866	1107	12(4)	0.92(40)	1.78(78)	$9^-/2 \rightarrow 5^-/2$	E2
773.1	3966	3193	61(9)	1.01(24)		$23^+/2 \rightarrow 19^+/2$	E2
774.0	4563	3789	<10			$(27^+/2) \rightarrow (27^+/2)$	$(M1/E2)$
774.2	5881	5107	<10			$(35^+/2) \rightarrow (31^+/2)$	(E2)

TABLE I. (Continued).

E_γ[a] (keV)	E_i (keV)	E_f (keV)	$I\gamma$[b]	$R_{\rm DCO}$[c]	$R_{\rm DCO}$[d]	$J_i^\pi \rightarrow J_f^\pi$	Multipolarity
784.0	2415	1631	11(3)	1.12(49)		$(13^+/2) \rightarrow (9^+/2)$	(E2)
787.4	4760	3973	30(7)		1.13(34)	$(29^-/2) \rightarrow (27^-/2)$	$(M1/E2)$
788.4	3072	2283	112(11)		1.02(19)	$19^+/2 \rightarrow 17^+/2$	$M1/E2$
803.7	3193	2390	77(13)	1.07(22)		$19^+/2 \rightarrow 15^+/2$	E2
807.5	3072	2264	17(5)		1.12(46)	$19^+/2 \rightarrow (17^+/2)$	$(M1/E2)$
818.2	5410	4592	34(7)	0.98(29)		$(31^-/2) \rightarrow (27^-/2)$	(E2)
826.2	4799	3973	<10			$(29^-/2) \rightarrow (27^-/2)$	$(M1/E2)$
835.1	4116	3280	19(2)		1.02(40)	$(27^-/2) \rightarrow (25^-/2)$	$(M1/E2)$
838.8	3122	2283	89(9)	0.98(20)		$21^+/2 \rightarrow 17^+/2$	E2
844.5	3868	3023	15(5)		1.05(44)	$(25^-/2) \rightarrow (23^-/2)$	$(M1/E2)$
844.2	3966	3122	<10			$23^+/2 \rightarrow 21^+/2$	$M1/E2$
882.6	5692	4809	<10			$(33^+/2) \rightarrow (29^+/2)$	(E2)
888.6	2233	1345	571(12)	0.60(5)		$(15^-/2) \rightarrow 13^+/2$	(E1)
894.4	5273	4378	17(5)		1.06(45)	$(31^+/2) \rightarrow (29^+/2)$	$(M1/E2)$
916.7	6230	5314	22(6)	1.01(40)		$(35^+/2) \rightarrow (31^+/2)$	$(E2)$
919.7	2264	1345	18(5)	1.03(42)	1.66(68)	$(17^+/2) \rightarrow 13^+/2$	$(E2)$
928.4	6338	5410	25(6)	0.97(35)		$(35^-/2) \rightarrow (31^-/2)$	$(E2)$
938.8	2283	1345	273(11)	0.99(13)		$17^+/2 \rightarrow 13^+/2$	$E2$
943.2	6050	5107	13(4)		1.71(75)	$(35^+/2) \rightarrow (31^+/2)$	$(E2)$
980.7	4378	3398	14(4)	1.09(46)	1.59(67)	$(29^+/2) \rightarrow (25^+/2)$	$(E2)$
987.0	6050	5063	<10			$(35^+/2) \rightarrow (31^+/2)$	$(E2)$
1014.4	3868	2854	13(4)		1.75(73)	$(25^-/2) \rightarrow (21^-/2)$	$(E2)$
1020.1	4809	3789	26(7)		0.95(32)	$(29^+/2) \rightarrow (27^+/2)$	$(M1/E2)$
1024.4	1024	0	23(6)	0.96(35)		$5^+/2 \rightarrow 9^+/2$	$(E2)$
1026.0	5457	4431	<10			$(31^-/2) \rightarrow (27^-/2)$	$(E2)$
1028.0	7366	6338	22(6)	1.12(42)		$(39^-/2) \rightarrow (35^-/2)$	$(E2)$
1039.0	5755	4715	10(3)		1.77(79)	$(33^-/2) \rightarrow (29^-/2)$	$(E2)$
1052.7	4841	3789	<10			$(29^+/2) \rightarrow (27^+/2)$	$(M1/E2)$
1061.1	7291	6230	24(6)	1.17(42)		$(39^+/2) \rightarrow (35^+/2)$	$(E2)$
1061.2	4459	3398	<10			$(25^+/2) \rightarrow (25^+/2)$	$(M1/E2)$
1097.9	2442	1345	31(7)		1.02(30)	$(15^-/2) \rightarrow 13^+/2$	$(E1)$
1104.7	5483	4378	<10			$(31^+/2) \rightarrow (29^+/2)$	$(M1/E2)$
1122.1	8488	7366	18(5)	1.07(43)		$(43^-/2) \rightarrow (39^-/2)$	$(E2)$
1147.6	8439	7291	17(5)	1.06(44)		$(43^+/2) \rightarrow (39^+/2)$	$(E2)$
1150.4	4431	3280	<10			$(27^-/2) \rightarrow (25^-/2)$	$(M1/E2)$
1152.2	5125	3973	15(5)		1.64(69)	$(31^-/2) \rightarrow (27^-/2)$	$(E2)$
1165.0	4563	3398	<20		0.84(34)	$(27^+/2) \rightarrow (25^+/2)$	$(M1/E2)$
1173.0	1173	0	41(9)		1.23(33)	$11^+/2 \rightarrow 9^+/2$	$M1/E2$
1191.5	1192	0	131(7)	0.62(12)		$7^+/2 \rightarrow 9^+/2$	$M1/E2$
1199.5	6708	5508	13(4)		1.77(78)	$(37^+/2) \rightarrow (33^+/2)$	$(E2)$
1207.2	4605	3398	24(6)		1.05(36)	$(27^+/2) \rightarrow (25^+/2)$	$(M1/E2)$
1212.0	9700	8488	13(4)	1.03(42)		$(47^-/2) \rightarrow (43^-/2)$	$(E2)$
1227.8	9667	8439	17(5)	1.05(43)		$(47^+/2) \rightarrow (43^+/2)$	$(E2)$
1242.0	5620	4378	<10			$(33^+/2) \rightarrow (29^+/2)$	$(E2)$
1244.4	4459	3214	14(4)		1.02(43)	$(25^+/2) \rightarrow (23^+/2)$	$(M1/E2)$
1271.0	10938	9667	10(3)	1.09(49)		$(51^+/2) \rightarrow (47^+/2)$	$(E2)$
1274.3	5063	3789	14(4)		1.65(70)	$(31^+/2) \rightarrow (27^+/2)$	$(E2)$
1276.7	5392	4116	<10			$(31^-/2) \rightarrow (27^-/2)$	$(E2)$
1294.0	10994	9700	10(3)	1.08(48)		$(51^-/2) \rightarrow (47^-/2)$	$(E2)$
1313.1	5692	4378	12(4)		1.68(73)	$(33^+/2) \rightarrow (29^+/2)$	$(E2)$
1318.1	5107	3789	31(8)		1.86(56)	$(31^+/2) \rightarrow (27^+/2)$	$(E2)$
1324.8	2669	1345	94(9)	1.10(22)		$17^+/2 \rightarrow 13^+/2$	$E2$
1336.5	4459	3122	<10			$(25^+/2) \rightarrow (21^+/2)$	$(E2)$
1344.5	1345	0	1000	1.01(5)	1.72(8)	$13^+/2 \rightarrow 9^+/2$	$E2$
1348.5	4563	3214	<!20		1.75(70)	$(27^+/2) \rightarrow (23^+/2)$	$(E2)$
1386.0	12380	10994	<10			$(55^-/2) \rightarrow (51^-/2)$	$(E2)$
1336.5	4459	3122	<10			$(25^+/2) \rightarrow (21^+/2)$	$(E2)$
1344.5	1345	0	1000	1.01(5)	1.72(8)	$13^+/2 \rightarrow 9^+/2$	$E2$

TABLE I. (Continued).

E_γ[a] (keV)	E_i (keV)	E_f (keV)	$I\gamma$[b]	$R_{\rm DCO}$[c]	$R_{\rm DCO}$[d]	$J_i^\pi \rightarrow J_f^\pi$	Multipolarity
1348.5	4563	3214	<20		1.75(70)	$(27^+/2) \rightarrow (23^+/2)$	$(E2)$
1386.0	12380	10994	<10			$(55^-/2) \rightarrow (51^-/2)$	$(E2)$
1390.7	4605	3214	17(5)		1.68(69)	$(27^+/2) \rightarrow (23^+/2)$	$(E2)$
1407.5	4431	3023	21(5)		1.68(67)	$(27^-/2) \rightarrow (23^-/2)$	$(E2)$
1411.2	4809	3398	<10			$(29^+/2) \rightarrow (25^+/2)$	$(E2)$
1419.3	5392	3973	16(5)		1.65(69)	$(31^-/2) \rightarrow (27^-/2)$	$(E2)$
1435.0	4715	3280	41(9)		1.59(43)	$(29^-/2) \rightarrow (25^-/2)$	$(E2)$
1443.7	4841	3398	13(4)		1.65(70)	$(29^+/2) \rightarrow (25^+/2)$	$(E2)$
1484.0	5273	3789	<10			$(31^+/2) \rightarrow (27^+/2)$	(E2)
1484.1	5457	3973	<10			$(31^-/2) \rightarrow (27^-/2)$	$(E2)$
1518.4	4799	3280	18(5)		1.71(70)	$(29^-/2) \rightarrow (25^-/2)$	$(E2)$
1584.5	2929	1345	24(6)	1.07(34)	1.67(58)	$(17^+/2) \rightarrow 13^+/2$	$(E2)$
1631.3	1631	0	<10			$(9^+/2) \rightarrow 9^+/2$	$(M1/E2)$
1694.4	5483	3789	11(4)		1.74(76)	$(31^+/2) \rightarrow (27^+/2)$	$(E2)$

[a]The uncertainty in strong γ-ray energies is less than 0.2 keV; for weak γ-ray energies, it is about 0.5 keV.
[b]Intensities are corrected for detector efficiency and normalized to 1000 for the 1344.5 keV transition.
[c]DCO ratios from a gate on the quadrupole transition.
[d]DCO ratios from a gate on the dipole transition.

obtained by gating on the 189 and 169 keV transitions, respectively. Additionally, the 484, 387, 396, and 844 keV linking transitions are of $\Delta I = 1$ character. The observation of $\Delta I = 1$ and $\Delta I = 2$ linking transitions between bands 2 and 4 implies that band 2 has negative parity as that of band 4. Furthermore, the DCO values of the intraband transitions of band 2 are consistent with $\Delta I = 1$ dipole character, and $E1$ multipolarity is unlikely, since $E1$ bands are connected with a static octupole deformation. There is no indication for that in this mass region. Hence the $M1/E2$ multipolarity is tentatively assigned to the intraband transitions of band 2. Based on above arguments, the spin-parity assignments of the levels in band 2 are proposed for the first time, as shown in Fig. 1.

Band 3 was determined to be a sequence of $\Delta I = 1$ γ transitions in Refs. [21,22]. In the present study, two new intraband transitions of 691 and 434 keV are observed and placed at the top of band 3, and the spin of this band is extended to $I^\pi = (47/2^-)$. The 298 keV transition is placed at the bottom of band 3 on the basis of the coincidence relationships, intensity balances, and energy sums, and thus the $I^\pi = (31/2^-)$ level of band 3 is tentatively assigned as the lowest observed state of this band. Moreover, several new linking transitions are found between bands 3 and 2, as well as between bands 3 and 4. The existence of these transitions further strengthens the placements and spin-parity assignments of the levels in band 3. A coincidence spectrum for the 341 keV transition from band 3 is shown in Fig. 2(a).

Band 7 is a positive-parity dipole band. The energies, intensities, and multipolarities of the intraband transitions obtained from the present data mostly agree with the previous works [22]. In addition, five new linking transitions of 419, 431, 1444, 1053, and 1484 keV between bands 7 and 8 are observed, and three new interband transitions of 373, 774, and 513 keV are identified between bands 7 and 9, so the excitation energies of band 7 are unambiguously fixed. A representative spectrum for these transitions is shown in Fig. 2(b), which depicts the spectrum gated by the 353 keV transition.

Band 8 consisting of a sequence of intense dipole transitions, was reported in Refs. [19–21]. This band is extended in the current work by two in-band 628 and 701 keV transitions. And two $E2$ crossover transitions within the band are observed, thereby confirming the ordering of the in-band dipole transitions up to the $(33/2^+)$ state. A sample spectrum is provided in Fig. 2(c).

Band 9 is characterized by strong $M1$ transitions and no $E2$ crossover transitions were observed in our early work [21]. In the present work, band 9 is extended to higher spin state by the addition of the 747 keV transition, and a 146 keV γ transition is also observed feeding out of the bottom of this band. Four new $E2$ crossover transitions of 502, 699, 943, and 1199 keV are found and firmly confirm the ordering of the dipole transitions of band 9. Moreover, eight new linking transitions of 1411, 774, 1391, 1061, 1244, 1336, 445, and 987 keV are observed to connect bands 9 to 8. A sample γ-γ coincidence spectrum supporting the level scheme is shown in Fig. 3(a). Multipolarity analysis indicates that the 1244 and 1391 keV linking transitions are of $\Delta I = 1$ and $\Delta I = 2$ character, respectively. Thus the spin and parity of the new lowest observed state of band 9 is deduced to be $I^\pi = (25/2^+)$, which also further supports the previous spin-parity assignments of this band [21].

Band 10, composed of quadrupole transitions, has previously been assigned positive parity via angular distribution analysis [19,20]. In the present experiment, two new intraband transitions of 1228 and 1271 keV are observed and placed at the top of this band. A sample spectrum is provided in Fig. 3(b). Multipolarity analysis indicates that the 1228 and 1271 keV transitions are of $\Delta I = 2$ character with DCO ratios of 1.05 and 1.09 obtained by gating on the quadrupole intraband transitions. Thus, the spins of band 10 are extended from $I^\pi = (43/2^+)$ to $I^\pi = (51/2^+)$, and $4\hbar$ higher than the earlier work. Meanwhile, a gentle up-band with the gain in

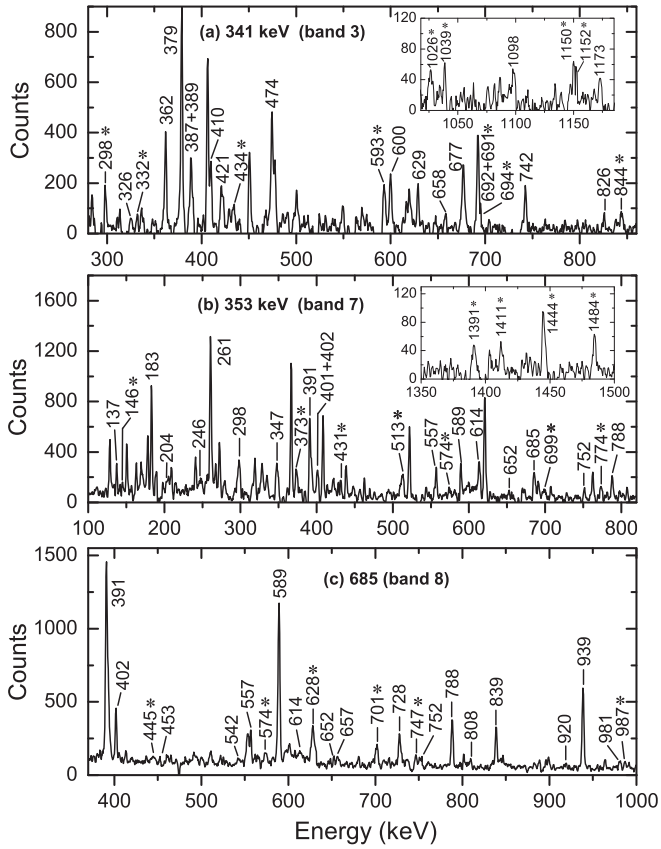

FIG. 2. γ-ray coincidence spectra with gates set on the (a) 341 keV, (b) 353 keV, and (c) 685 keV transitions, among them (a) from 50 MeV experiment, (b) and (c) from 38 MeV experiment. Insets show the higher-energy part of the spectra. The newly identified γ rays are marked with the asterisks.

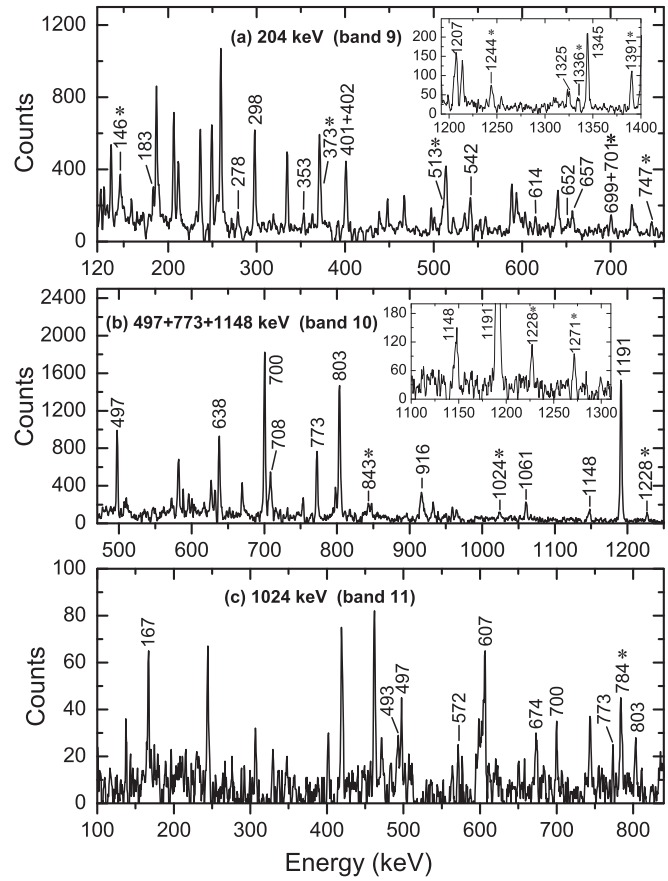

FIG. 3. γ-ray coincidence spectra with gates set on the (a) 204 keV, (b) $497 + 773 + 1148$ keV, and (c) 1024 keV transitions, among them (a) and (c) from 38 MeV experiment, (b) from 50 MeV experiment. Insets show the higher-energy part of the spectra. The newly identified γ rays are marked with the asterisks.

aligned angular momentum of about $4\hbar$ after the back-bend is observed in band 10. The details of this band are discussed in the later section.

Band 11 is a newly observed rotational band built on the previously known $5/2^+$ state at 1024 keV, and decays to the ground state ($I^\pi = 9/2^+$) via two linking transitions with energies of 1631 and 1024 keV. Figure 3(c) shows the spectrum gated by the 1024 keV γ transition. Multipolarity analysis indicates that the 607 and 784 keV intraband transitions are of $\Delta I = 2$ character with DCO ratios of 1.04 and 1.12 obtained by gating on the 1024 keV transition, respectively. Thus, band 11 is suggested as a positive parity $\Delta I = 2$ band as that of band 10.

IV. DISCUSSION

Previously, the bands 1–9 have been discussed in our early works [21,22], in which the $\Delta I = 1$ bands have been suggested as magnetic rotational bands based on the experimental research and theoretical calculation. In the current paper, the following discussion is mainly focused on the $\Delta I = 2$ bands 10 and 11.

The positive-parity band 10 is due to the proton one-particle-one-hole ($1p$-$1h$) excitation across the $Z = 50$ shell gap, the underlying configuration being $\pi g_{9/2}^{-2} g_{7/2}$ [19]. To further interpret this structure, the observed spins I of band 10 are plotted in Fig. 4 as a function of rotational frequency ω, where $\hbar\omega(I) = [E(I) - E(I-2)]/2$. In Fig. 4, a sharp back-bend is observed around $\hbar\omega \approx 0.4$ MeV due to the alignment of the two $h_{11/2}$ neutrons, being the lowest band crossing in this mass region, and implies a weak interaction between the aligned and the nonaligned structures [23,24]. Immediately, after the back-bend, there is again a gentle up-bend at frequencies greater than $\approx$0.6 MeV/$\hbar$ with the gain in aligned angular momentum of about $4\hbar$, which is probably attributed to the alignment of neutrons in the positive-parity $\nu g_{7/2}/d_{5/2}$ orbitals. Because of the $g_{7/2}$ valence proton and aligned neutrons occupy similar $\nu g_{7/2}/d_{5/2}$ orbitals, leading to a large overlap between the neutron and proton wave functions. Hence, the alignment of $\nu g_{7/2}/d_{5/2}$ neutrons may be particularly influenced by a residual proton-neutron interaction [23,24], which possibly accounts for the observed gentle up-bend in band 10. Considering the properties mentioned above, we suggest that the band 10 of ^{113}In has a three-quasiparticle $\pi g_{9/2}^{-2} g_{7/2}$ configuration before the sharp back-bend and a five-quasiparticle $\pi g_{9/2}^{-2} g_{7/2} \otimes \nu(h_{11/2})^2$

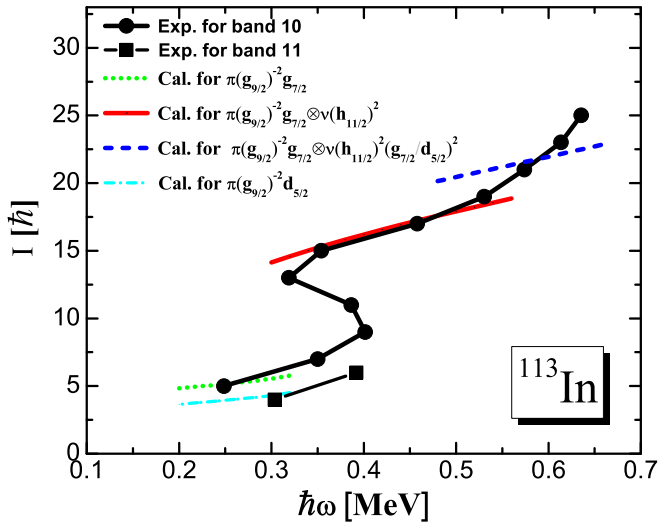

FIG. 4. Angular momentum as a function of rotational frequency for bands 10 and 11 in ^{113}In in comparison with the corresponding TAC-RMF calculations for the suggested configurations.

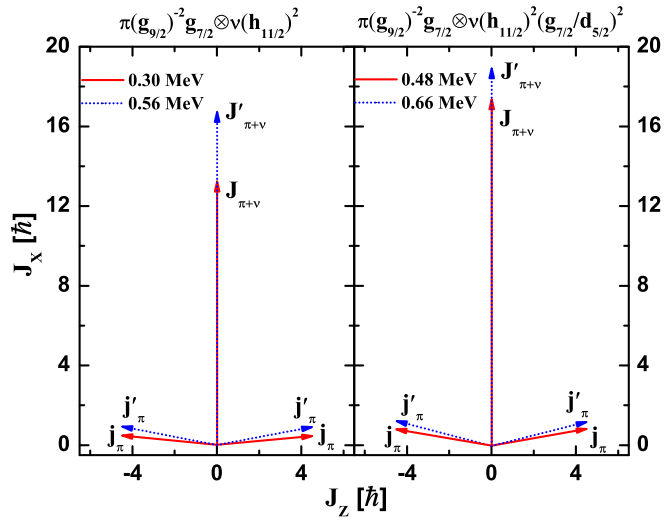

FIG. 5. Angular momentum vectors of neutrons and the low-Ω $g_{7/2}$ proton particle, $J_{\pi+\nu}$, together with two high-Ω $g_{9/2}$ proton holes, j_π.

configuration after the back-bend, and a gentle up-bend is attributed to the $\pi g_{9/2}^{-2} g_{7/2} \otimes \nu(h_{11/2})^2 (g_{7/2}/d_{5/2})^2$ configuration.

To further confirm the configuration assignment of band 10 and investigate corresponding rotation mechanism, the self-consistent tilted axis cranking relativistic mean-field (TAC-RMF) model has been performed. So far, the TAC-RMF model has been applied successfully to describe the antimagnetic rotational bands in ^{105}Cd [25], ^{109}Cd [26], ^{110}Cd [27], ^{108,110}In [28], and ^{112}In [16]. In the present calculations, the self-consistent two-dimensional cranking RMF theory with parameter set PC-PK1 [29] is used, while the pairing correlations are neglected. In Fig. 4, the experimental angular momentum as a function of frequency for band 10 is compared with TAC-RMF calculations for the proposed configurations. As can be seen in Fig. 4, the calculations are in general agreement with the trend of experimental angular momentum of band 10, supporting the configuration assignment of this band. The small discrepancy between the experimental data and the calculations might be due to the pairing correlation, which is not considered in this TAC-RMF calculations. Taking the pairing correlation into account might improve the result, as discussed in Ref. [30].

In this mass region, the high-Ω $g_{9/2}$ proton holes and low-Ω $h_{11/2}$ neutrons are known to play an active role in the antimagnetic rotation [1]. Indeed, these basic condition for the occurrence of antimagnetic rotation can be met in the positive-parity band 10. Thus, it would be interesting to study whether the properties of band 10 can be described by the two-shears-like mechanism.

In order to examine the possible two-shears-like mechanism in band 10, the total angular momentum vector of neutrons and the low-Ω $g_{7/2}$ proton particle, $J_{\pi+\nu}$, and the two high-Ω $g_{9/2}$ proton holes, j_π, were calculated similarly as in Refs. [25,31]. The calculated results for the $\pi g_{9/2}^{-2} g_{7/2} \otimes \nu(h_{11/2})^2$ configuration after the back-bend, along with a gentle up-bend with the configuration of $\pi g_{9/2}^{-2} g_{7/2} \otimes \nu(h_{11/2})^2 (g_{7/2}/d_{5/2})^2$ are presented in Fig. 5. It is clear from Fig. 5 that the two proton angular momentum vectors j_π are pointing opposite to each other and nearly perpendicular to the angular momentum vector $J_{\pi+\nu}$ at the beginning frequency. They form the blades of the two shears. As the rotational frequency increases, the vectors j_π of the two $g_{9/2}$ proton holes gradually align toward the vector $J_{\pi+\nu}$, the direction of the total angular momentum is almost unchanged. It presents a picture of the two shears closing simultaneously by moving one blade toward the other. In such a way, the two-shears-like mechanism in ^{113}In is clearly demonstrated in Fig. 5.

Typical characteristics of antimagnetic rotation include weak $E2$ transitions, a decrease of the $B(E2)$ values with increasing spin, and a large $J^{(2)}/B(E2)$ ratio [$\approx$100 MeV$^{-1}\hbar^2(eb)^{-2}$] [1,6]. In Fig. 6, the calculated $B(E2)$ values and the $J^{(2)}/B(E2)$ ratios are shown as functions of the rotational frequency in the TAC-RMF calculations for the assigned configurations. As can be seen from Fig. 6, the $B(E2)$ values decrease smoothly with increasing rotational frequency for both assigned configurations. Furthermore, the calculated $J^{(2)}/B(E2)$ ratios for the configurations above mentioned are around 100 MeV$^{-1}\hbar^2(eb)^{-2}$, which are much higher than 10 MeV$^{-1}\hbar^2(eb)^{-2}$ for well deformed heavy nuclei and 5 MeV$^{-1}\hbar^2(eb)^{-2}$ for superdeformed nuclei [1]. These calculated results are consistent with the characteristics of the two-shears-like mechanism.

The decrease of the $B(E2)$ values can be understood by the changes in the nuclear deformation. In Fig. 7, we present the evolution of the deformation for the $\pi g_{9/2}^{-2} g_{7/2} \otimes \nu(h_{11/2})^2$ and $\pi g_{9/2}^{-2} g_{7/2} \otimes \nu(h_{11/2})^2 (g_{7/2}/d_{5/2})^2$ configurations in the (β_2, γ) plane with increasing rotational frequency. As shown in Fig. 7, for both assigned configurations, the β_2 deformations gradually decrease with the rotational frequency, and the β_2 and γ values are smaller. It indicates that the nucleus

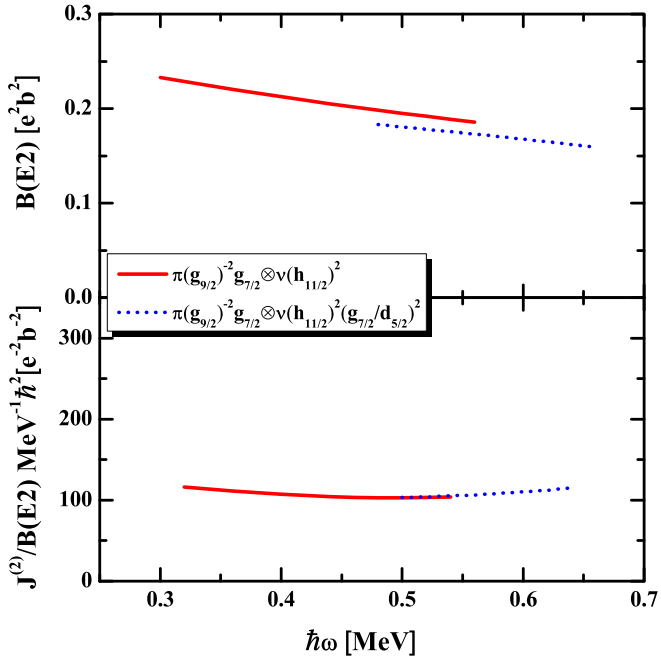

FIG. 6. Calculated $B(E2)$ values and $J^{(2)}/B(E2)$ ratios for the $\pi g_{9/2}^{-2} g_{7/2} \otimes \nu(h_{11/2})^2$ and $\pi g_{9/2}^{-2} g_{7/2} \otimes \nu(h_{11/2})^2 (g_{7/2}/d_{5/2})^2$ configurations in ^{113}In

^{113}In is a weakly deformed nucleus, which is one of the basic conditions for the occurrence of antimagnetic rotation.

As mentioned above, the features of the positive-parity band 10, based on the $\pi g_{9/2}^{-2} g_{7/2} \otimes \nu(h_{11/2})^2$ configuration after the back-bend and the $\pi g_{9/2}^{-2} g_{7/2} \otimes \nu(h_{11/2})^2 (g_{7/2}/d_{5/2})^2$ configuration with a gentle up-bend, generally conform to the fingerprints of antimagnetic rotation. However, to confirm this suggestion, the further experimental results of absolute $B(E2)$ transition probabilities based on lifetime measurements are desirable to reach a definitive conclusion.

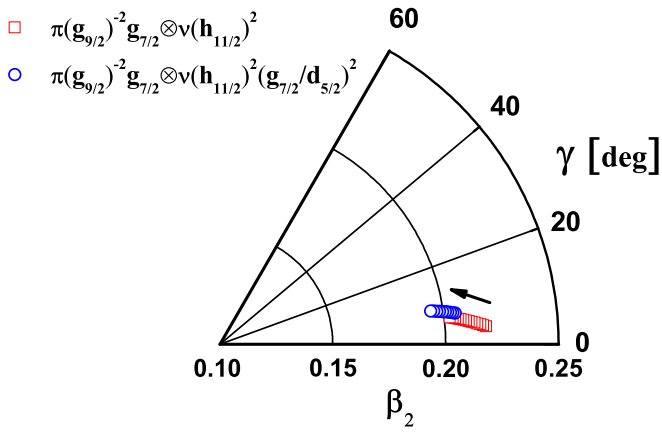

FIG. 7. Evolutions of deformation in the (β_2, γ) plane with rotational frequency in the TAC-CDFT calculations. The rotational frequencies increase from 0.30–0.56 MeV and from 0.48–0.66 MeV corresponding to the $\pi g_{9/2}^{-2} g_{7/2} \otimes \nu(h_{11/2})^2$ and $\pi g_{9/2}^{-2} g_{7/2} \otimes \nu(h_{11/2})^2 (g_{7/2}/d_{5/2})^2$ configurations, respectively.

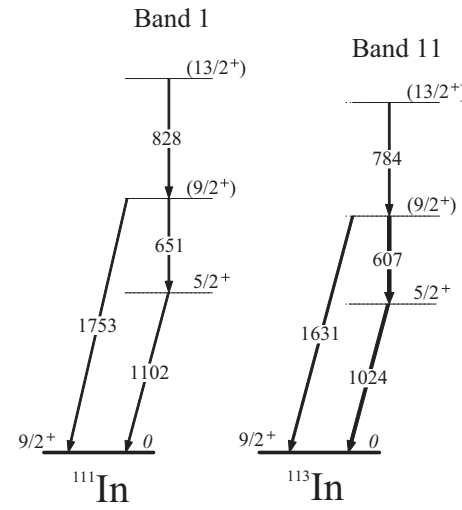

FIG. 8. Systematic comparison of the $\pi g_{9/2}^{-2} \otimes \pi d_{5/2}$ bands in ^{111}In [32] and ^{113}In.

Band 11 decaying to the ground state is observed for the first time. Considering the Fermi surface for both protons and neutrons of the ^{113}In nucleus, the $5/2^+$ state of band 11 at 1102 keV may be viewed as an intruder $1p2h$ state of predominantly $\pi d_{5/2}$ character. Indeed, the $(9/2^+)$ and $(13/2^+)$ levels of band 11 could belong to a rotational band built on this state. Moreover, the similar structure has also been observed in neighboring ^{111}In nucleus [32]. For comparison, the level scheme of band 1 in ^{111}In, and that of band 11 in ^{113}In are presented in Fig. 8. One can see from Fig. 8 that both bands show very similar behavior, including the decay pattern and the excitation energy. It indicates that such two nuclei may be similar in nature, and the band 1 in ^{111}In has previously been suggested to the $\pi d_{5/2}$ configuration. Hence, it is reasonable that band 11 of ^{113}In has the same configuration as that of band 1 in ^{111}In. To further confirm the configuration assignment of band 11 in ^{113}In, the experimental angular momentum as a function of frequency for band 11 is compared with TAC-RMF calculations for the proposed configuration in Fig. 4. Calculated values show a reasonable agreement with the experimental data, supporting the configuration assignment of band 11 in ^{113}In. But because of its limited extent, the detailed rotational characteristics of this band cannot be analyzed further.

V. SUMMARY

The high-spin states of ^{113}In are reinvestigated via two experiments. The previously established level scheme of ^{113}In has been extended by the addition of about 50 new transitions. The spin-parity assignments of the levels in band 2 are proposed for the first time. Three known $\Delta I = 1$ bands are extended to higher spin states, and several new in-band quadrupole crossover transitions are observed in two of the dipole bands. A number of new interband transitions are identified, further confirming the level structures and spin-

parity assignments in ^{113}In. Moreover, a new $\Delta I = 2$ band is observed. It is interpreted as a rotational structure built on the $1p$-$1h$ proton excitation from the $\pi g_{9/2}$ to the $\pi d_{5/2}$ orbital. The previously observed positive-parity $\Delta I = 2$ band is extended to $(51/2^+)$ state, and a gentle up-bend associated to the alignment of neutrons in the $\nu g_{7/2}/d_{5/2}$ orbitals is identified. Based on the self-consistent tilted axis cranking relativistic mean-field model calculations, the predicted $B(E2)$, deformation parameters β_2 and γ, and $J^{(2)}/B(E2)$ ratios are discussed for the $\pi g_{9/2}^{-2} g_{7/2} \otimes \nu(h_{11/2})^2$ and $\pi g_{9/2}^{-2} g_{7/2} \otimes \nu(h_{11/2})^2 (g_{7/2}/d_{5/2})^2$ structures, and the properties of these two structures show general agreement with the fingerprints of two-shears-like mechanism. Thus, both structures are suggested to be the candidate antimagnetic rotational bands in ^{113}In. However, to confirm this suggestion, the further experimental results of absolute $B(E2)$ transition probabilities based on lifetime measurements are desirable.

ACKNOWLEDGMENTS

This work is supported by the National Natural Science Foundation of China under Grants No. 11775098, No. 11475072, No. 11675063, No. U1867210, No. 11405072, No. 11205069, and No. 11075064, Jilin Scientific and Technological Development Programs No. 20190201137JC and No. 20180520195JH, the 13th Five-Year Plan of Scientific Research of Jilin Province No. JJKH20180117KJ, China Postdoctoral Science Foundation No. 2015M571354 and No. 2013M541285, the National Basic Research Programme of China under Grant No. 2007CB815005, and the Fundamental Research Funds for the Central Universities.

[1] S. Frauendorf, Rev. Mod. Phys. **73**, 463 (2001).
[2] D. Choudhury, A. K. Jain, M. Patial, N. Gupta, P. Arumugam, A. Dhal, R. K. Sinha, L. Chaturvedi, P. K. Joshi *et al.*, Phys. Rev. C **82**, 061308(R) (2010).
[3] A. J. Simons, R. Wadsworth, D. G. Jenkins, R. M. Clark, M. Cromaz, M. A. Deleplanque, R. M. Diamond, P. Fallon, G. J. Lane *et al.*, Phys. Rev. Lett. **91**, 162501 (2003).
[4] D. Choudhury, A. K. Jain, G. A. Kumar, S. Kumar, S. Singh, P. Singh, M. Sainath, T. Trivedi, J. Sethi *et al.*, Phys. Rev. C **87**, 034304 (2013).
[5] A. J. Simons, R. Wadsworth, D. G. Jenkins, R. M. Clark, M. Cromaz, M. A. Deleplanque, R. M. Diamond, P. Fallon, G. J. Lane *et al.*, Phys. Rev. C **72**, 024318 (2005).
[6] P. Datta, S. Chattopadhyay, S. Bhattacharya, T. K. Ghosh, A. Goswami, S. Pal, M. Saha Sarkar, H. C. Jain, P. K. Joshi *et al.*, Phys. Rev. C **71**, 041305(R) (2005).
[7] C. J. Chiara, S. J. Asztalos, B. Busse, R. M. Clark, M. Cromaz, M. A. Deleplanque, R. M. Diamond, P. Fallon, D. B. Fossan *et al.*, Phys. Rev. C **61**, 034318 (2000).
[8] S. Roy, S. Chattopadhyay, P. Datta, S. Pal, S. Bhattacharya, R. K. Bhowmik, A. Goswami, H. C. Jain, R. Kumar, S. Muralithar *et al.*, Phys. Lett. B **694**, 322 (2011).
[9] S. Zhu, U. Garg, A. V. Afanasjev, S. Frauendorf, B. Kharraja, S. S. Ghugre, S. N. Chintalapudi, R. V. F. Janssens, M. P. Carpenter *et al.*, Phys. Rev. C **64**, 041302(R) (2001).
[10] M. Sugawara, T. Hayakawa, M. Oshima, Y. Toh, A. Osa, M. Matsuda, T. Shizuma, Y. Hatsukawa, H. Kusakari *et al.*, Phys. Rev. C **92**, 024309 (2015).
[11] M. Sugawara, T. Hayakawa, M. Oshima, Y. Toh, A. Osa, M. Matsuda, T. Shizuma, Y. Hatsukawa, H. Kusakari, T. Morikawa *et al.*, Phys. Rev. C **86**, 034326 (2012).
[12] V. Singh, S. Sihotra, S. Roy, M. Kaur, S. Saha, J. Sethi, R. Palit, N. Singh, S. S. Malik *et al.*, J. Phys. (London) G **44**, 075105 (2017).
[13] N. Rather, S. Roy, P. Datta, S. Chattopadhyay, A. Goswami, S. Nag, R. Palit, S. Pal, S. Saha *et al.*, Phys. Rev. C **89**, 061303(R) (2014).
[14] N. Rather, P. Datta, S. Chattopadhyay, A. Gowsami, S. Nag, S. Roy, R. Palit, S. Saha, J. Sethi, and T. Trivedi, Proc. DAE Symp. Nucl. Phys. **59**, 108 (2014).
[15] C. J. Chiara, D. B. Fossan, V. P. Janzen, T. Koike, D. R. LaFosse, G. J. Lane, S. M. Mullins, E. S. Paul, D. C. Radford *et al.*, Phys. Rev. C **64**, 054314 (2001).
[16] X. W. Li, J. Li, J. B. Lu, K. Y. Ma, Y. H. Wu, L. H. Zhu, C. Y. He, X. Q. Li, Y. Zheng *et al.*, Phys. Rev. C **86**, 057305 (2012).
[17] J. Sethi, R. Palit, S. Saha, D. Choudhury, T. Trivedi, S. Biswas, P. Singh, H. C. Jain, S. Kumar *et al.*, Proc. DAE Symp. Nucl. Phys. **59**, 118 (2014).
[18] K. S. Krane, R. M. Steffen, and R. M. Wheeler, Nucl. Data Tables A **11**, 351 (1973).
[19] R. S. Chakrawarthy and R. G. Pillay, Phys. Rev. C **55**, 155 (1997).
[20] S. Naguleswaran, R. S. Chakrawarthy, U. Garg, K. L. Lamkin, G. Smith, J. C. Walpe, A. Galindo-Uribarri, V. P. Janzen, D. C. Radford *et al.*, Phys. Rev. C **72**, 044304 (2005).
[21] K. Y. Ma, J. B. Lu, D. Yang, H. D. Wang, Y. Z. Liu, J. Li, L. H. Zhu, X. G. Wu, Y. Zheng, and C. Y. He, Eur. Phys. J. A **48**, 82 (2012).
[22] K. Y. Ma, J. B. Lu, D. Yang, J. Li, H. D. Wang, Y. Z. Liu, X. G. Wu, L. H. Zhu, Y. Zheng, and C. Y. He, Chin. Phys. Lett. **29**, 062102 (2012).
[23] V. P. Janzen, H. R. Andrews, B. Haas, D. C. Radford, D. Ward, A. Omar, D. Prevost, M. Sawicki, P. Unrau *et al.*, Phys. Rev. Lett. **70**, 1065 (1993).
[24] R. A. Wyss and A. Johnson, in *Proceedings of the International Conference on High Spin Physics and Gamma Soft Nuclei* (World Scientific, Singapore, 1991), p. 123.
[25] P. W. Zhao, J. Peng, H. Z. Liang, P. Ring, and J. Meng, Phys. Rev. Lett. **107**, 122501 (2011).
[26] P. Zhang, B. Qi, and S. Y. Wang, Phys. Rev. C **89**, 047302 (2014).
[27] J. Peng and P. W. Zhao, Phys. Rev. C **91**, 044329 (2015).
[28] W. J. Sun, H. D. Xu, J. Li, Y. H. Liu, K. Y. Ma, D. Yang, J. B. Lu, and Y. J. Ma, Chin. Phys. C **40**, 084101 (2016).
[29] P. W. Zhao, Z. P. Li, J. M. Yao, and J. Meng, Phys. Rev. C **82**, 054319 (2010).
[30] P. W. Zhao, S. Q. Zhang, and J. Meng, Phys. Rev. C **92**, 034319 (2015).
[31] P. W. Zhao, J. Peng, H. Z. Liang, P. Ring, and J. Meng, Phys. Rev. C **85**, 054310 (2012).
[32] P. Vaska, D. B. Fossan, D. R. LaFosse, H. Schnare, M. P. Waring, S. M. Mullins, G. Hackman, D. Prevost, J. C. Waddington *et al.*, Phys. Rev. C **57**, 1634 (1998).